Key Points:
- Extent of the highlands consistent with that observed on the map of Mars
- Decline time of the volcanism consistent with geological observations
- Decline time of the transient magnetic field consistent with the observations

Correspondence to:
G. Leone,
giovanni.leone@erdw.ethz.ch

Three-dimensional simulations of the southern polar giant impact hypothesis for the origin of the Martian dichotomy

Giovanni Leone[1], Paul J. Tackley[1], Taras V. Gerya[1], Dave A. May[1], and Guizhi Zhu[1]

[1]Institute of Geophysics, ETH Zurich, Zurich, Switzerland

Abstract We demonstrate via numerical simulations that the impact of a ~lunar-sized body with Mars is capable of creating a hemispherical magma ocean that upon cooling and solidification resulted in the formation of the southern highlands and thus the Martian dichotomy. The giant impact may have contributed a significant amount of iron to the Martian core and generated a deep thermal anomaly that led to the onset and development of the volcanism in the southern highlands. Our model predicts several mantle plumes converging to the South Pole from the equatorial regions as well as new plumes forming in the equatorial region and also an absence of significant large-scale volcanism in the northern lowlands. The core heat flux evolution obtained from our numerical models is consistent with the decline of the magnetic field. We argue that such a scenario is more consistent with a range of observations than a northern giant impact (excavating the Borealis basin) for the formation of the Martian dichotomy.

1. Introduction

Previous studies have suggested that the Martian dichotomy may have been generated either by endogenic processes like degree-1 mantle convection [*Keller and Tackley*, 2009; *Zhong and Zuber*, 2001] or by exogenic (impact) processes: multiple impacts in the northern hemisphere [*Frey and Schultz*, 1988], or a giant impact occurring on the northern hemisphere of the planet forming the Borealis basin [*Andrews-Hanna et al.*, 2008; *Marinova et al.*, 2008; *Nimmo et al.*, 2008; *Wilhelms and Squyres*, 1984]. However, these hypotheses have several problems in particular: (i) despite the apparent difference in cratering rates between highlands and lowlands, the quasi-circular depressions in the lowlands hint at a similar crustal age for both hemispheres [*Frey*, 2006], which are estimated to start formation during or immediately after the planet's accretion; therefore, the crustal dichotomy is the most ancient geologic feature on the planet [*Solomon et al.*, 2005; *Carr and Head*, 2010]; (ii) multiple impacts occurring only on the northern hemisphere to shape the lowlands are statistically unlikely; (iii) impacts as large as those proposed for the formation of the Borealis basin [*Andrews-Hanna et al.*, 2008; *Marinova et al.*, 2008; *Nimmo et al.*, 2008] tend to create a deep thermal anomaly, upwelling, and magmatism that continues for a much longer time period than the initial impact-generated magma, inconsistent with both topography and the evident lack of significant volcanic edifices in the northern lowlands [*Tanaka et al.*, 2008].

An alternative hypothesis to the Northern Polar Giant Impact is that a Southern Polar Giant Impact (SPGI) with a body between 0.1 and 1.0 lunar masses (≈800–1700 km radius) generated a hemispherical magma ocean (the Australis magma ocean) that solidified to form the thicker crust of the southern hemisphere, as already investigated analytically [*Reese and Solomatov*, 2006, 2010; *Reese et al.*, 2011]. The resulting mantle thermal anomaly may also have induced degree-1 convection leading to further magmatism in the southern hemisphere, something that the analysis of *Reese and Solomatov* [2006, 2010] and *Reese et al.* [2011] did not cover. *Golabek et al.* [2011] tested this hypothesis using a suite of 2-D numerical simulations going from the immediate postimpact time to the present day, finding that it is indeed a viable hypothesis. However, since the formation of the dichotomy is an inherently 3-D process [*Keller and Tackley*, 2009], we have conducted a series of 3-D simulations of postgiant impact evolution of a Mars-sized planet.

2. Method

The physical principles and assumptions adopted in these 3-D experiments are essentially the same as those in the previous 2-D experiments [*Golabek et al.*, 2011]. We used the I3ELVIS code [*Gerya and Yuen*, 2007]
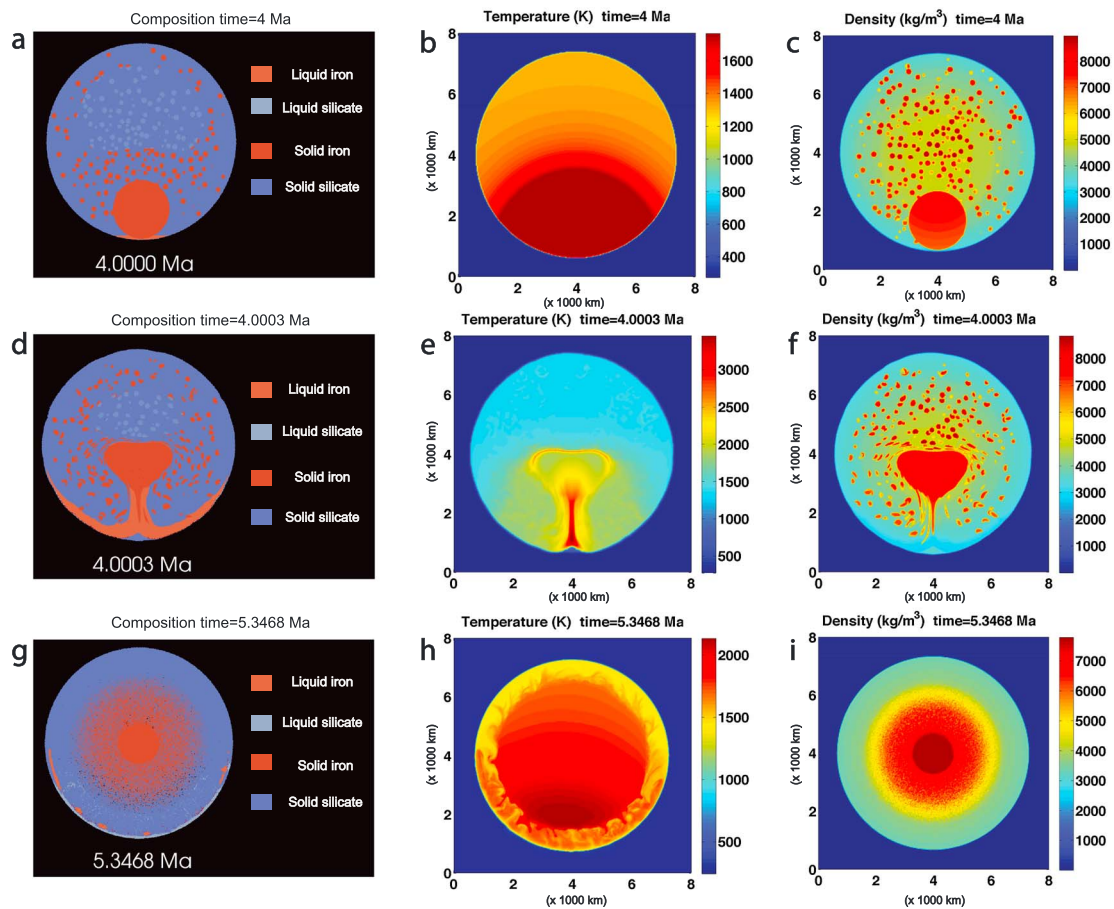
Figure 1. (a, d, and g) Composition, (b, e, and h) temperature, and (c, f, and i) density fields for the immediate postimpact time and for the postimpact period, the numbers from 0 to 8 on each axis of the temperature and density fields refer to the model box (8000 km). Figures 1a–1c are at the giant impact time of 4 Ma after CAI; Figures 1d–1f are at 4.0003 Ma after CAI; Figures 1g–1i are at 5.3468 Ma after CAI. The colored rectangles for the composition field shows a scale where the colors indicate the specific material type used within the I3ELVIS program: 5 (blue) is solid silicate, 10 (pale blue) is molten silicate metal, 25 (pale red) is molten iron, and 30 (red) is solid iron. In Figure 1g, the molten phases are mixed together because the differentiation process is still in its initial phase, so that it is quite difficult to discern them, particularly in the inner part of the planet. The small red circles in Figures 1a, 1c, 1d, and 1f are the iron cores of smaller impactors that hit the planet before the giant impact.

to simulate in 3-D the period immediately following the giant impact. We then used the StagYY code [*Tackley*, 2008] to simulate the long-term evolution over 4.5 Ga to the present day, including mantle convection, crustal growth, and core-mantle boundary (CMB) and surface heat flux. This involved the transfer of temperature and composition fields from I3ELVIS to StagYY. A detailed description of the numerical modeling methods and model parameters is given in the supporting information.

The effect of the impact is parameterized as in the previous 2-D study [*Golabek et al.*, 2011] and based on earlier works [*Tonks and Melosh*, 1993; *Senshu et al.*, 2002; *Monteux et al.*, 2007; *Reese et al.*, 2010]. The impactor is assumed to have hit the South Pole and to have caused an increase of pressure, such that a spherical region underneath the impact point had maximum pressure (an isobaric core [*Osinski and Pierazzo*, 2013]), beyond which the pressures rapidly dropped (Figure 1b) [*Golabek et al.*, 2011]. As in the 2-D research, the impact is assumed to have happened when the planet was fully accreted but not yet differentiated (Figure 1a). The impactor's core is placed at the base of the heated region (Figure 1b). Regarding impact velocity, previous estimates suggested 50% planet surface melting in case of an impactor/target mass ratio of 0.14 at a speed of 15 km s^{-1} [*Tonks and Melosh*, 1993], but N-body simulations have shown that the impactors' speed is more frequently just slightly larger than the escape velocity of the target [*Agnor et al.*, 1999] and rarely more than twice the escape velocity. Mars' escape velocity of 5 km s^{-1} is also slow enough to avoid bouncing or disruption processes during the giant impact [*Stewart and Leinhardt*, 2012]. Oblique

impacts were not considered because they are less effective than vertical ones, i.e., the volume of produced impact melt decreases rapidly with impact angle [*Leinhardt and Richardson*, 2002; *Pierazzo and Melosh*, 2000; *Reese and Solomatov*, 2010]. The effect of higher impact velocities of up to $10\,km\,s^{-1}$ [*Le Feuvre and Wieczorek*, 2008] with smaller impactors was instead explored; N-body simulations of terrestrial planet formation indicate that this is not yet at the upper end of the likely range of velocities for Mars but that it is statistically less likely than the escape velocity [*Agnor et al.*, 1999; *Morishima et al.*, 2010].

We have performed our 3-D runs for impactor sizes ranging from 1008 to 2000 km radius (instead of the ~400–1000 km in the 2-D experiments), focusing on mesosiderite-type composition (50% iron by radius) but also including a case with siderite composition (80% iron in radius) and a case with a pure stony impactor. We neglected nickel because its average 7–15 wt % [*McCoy et al.*, 2011] in impactors' cores makes negligible difference to our results. The higher iron content case is interesting because of the presence of M-type asteroids like 16 Psyche as well as several others in the asteroid belt [*Ockert-Bell et al.*, 2010], which are likely remnants of larger parent bodies in the 1–2 AU range that migrated in the current position after giant impacts with protoplanets [*Goldstein et al.*, 2009].

We tested impact times from 0 to 5 Ma after calcium-aluminium-rich Inclusions (CAI), when impactors up to Moon-size were already available [*Agnor et al.*, 1999], then settled on an impact time of 4 Ma (the 2-D experiments used 5 Ma), when radiogenic heating was weaker than during accretion due to the decay of the short-lived radionuclides (^{26}Al and ^{60}Fe) and the Martian core was not yet completely formed [*Sramek et al.*, 2012]. This value is also above the earliest time of 3 Ma indicated by the geochemistry [*Jacobsen*, 2005] but still within an upper bound that places the core formation around 15 Ma [*Righter and Shearer*, 2003]. Later additions to the core are not precluded if the new impactors' cores merge quickly without equilibrating with the silicate part of the planet, although an impactor of the size considered here might cause significant reequilibration. The short-lived radiogenic heating is strong until 3 Ma so that any newly formed crust would be remelted. Newly formed crust is stable from 4 Ma onward when this effect decays.

3. Results

Here we present all cases. The effects of varying impactor size, velocity, and composition are also discussed. Our best cases are a mesosiderite (50% iron by radius) of 2000 km radius (Figure S2 in the supporting information) and a siderite (80% iron by radius) of 1600 km radius, both with an impact speed of $5\,km\,s^{-1}$ (Figure S1).

Figure 1 shows the processes of core formation and massive melting in the impact hemisphere for the 2000 km mesosideritic impactor, also shown in the supporting information Movie S1, while supporting information Movie S2 shows the development of the mantle plumes for the 1600 km sideritic impactor. The impactor's core reaches the planet's center and merges with the planet's forming core (Figures 1d–1f), resulting in a differentiated structure of the planet. After 1.3 Ma postimpact, pockets of partially molten silicate are still visible beneath the cooled crust (Figure 1g), while the halo around the core is formed by incomplete differentiation of the iron from the silicate. Core formation occurs very rapidly—in our simulations, the planet's core is formed by ~5 Ma after CAI (Figures 1g–1i), i.e., about 1 Ma after the impact. However, it could be that even shorter timescales are realistic, which are here not resolved due to the applied minimum viscosity cutoff (see supporting information). A larger mesosideritic impactor (2000 km radius, 50% iron by radius, and impact speed $5\,km\,s^{-1}$) produces a hemispherical magma ocean consistent with the extent of the Martian dichotomy (Figures 1g–2a). For comparison, in the 2-D experiments [*Golabek et al.*, 2011], a much smaller impactor (1000 km radius, 50% iron by radius, and $5\,km\,s^{-1}$) produced a hemispherical dichotomy—this difference can be understood because the important criterion is the ratio of impactor kinetic energy (which is proportional to impactor mass) to planet mass: in 2-D this scales as $(r_{impactor}/r_{planet})^2$ whereas in 3-D it scales as $(r_{impactor}/r_{planet})^3$; thus, in 3-D a larger impactor is required. A smaller, mesosideritic, 1600 km diameter impactor is less efficient in producing a dichotomy (Figures 2c and 2d), although additional iron in its core would increase the shear heating and thus the extent of the magma ocean (Figure S1). Increasing the impact velocity while decreasing the radius such as to maintain a constant kinetic energy produced almost the same extent of thickened crust, both for a 1221 km (radius) mesosiderite at $7.5\,km\,s^{-1}$ and for a 1008 km mesosiderite at $10\,km\,s^{-1}$ (Figures 2e and 2f and Figures 2g and 2h, respectively). A stony impactor of 1750 km radius at $5\,km\,s^{-1}$ was less effective (Figures 2i and 2j). At $5\,km\,s^{-1}$, an
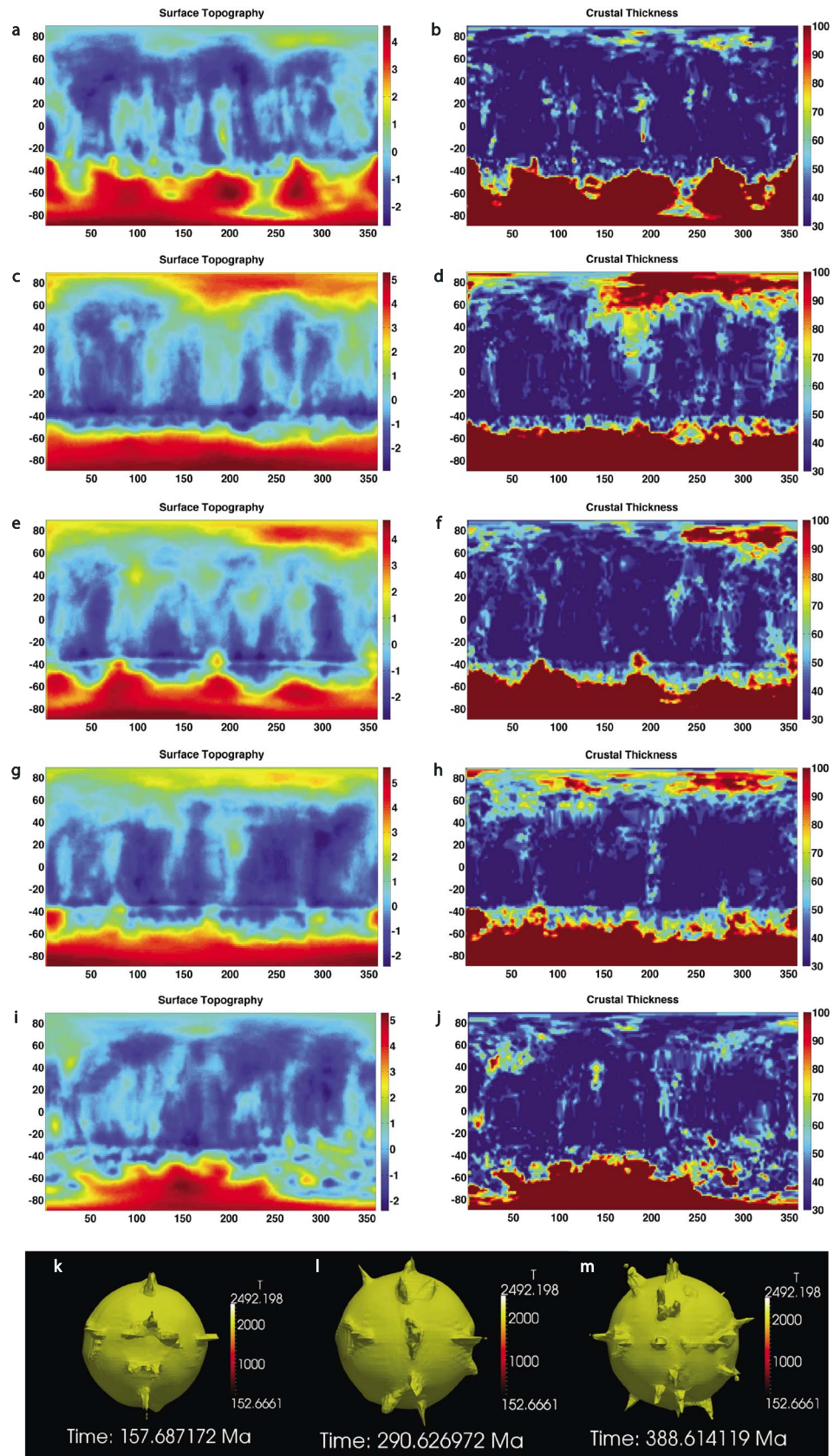
Figure 2

impactor radius of 2000 km is required in order to reasonably match the latitude of the highlands with a mesosideritic impactor (Figures 2a and 2b). Our results for both the 2000 km and 1600 km impactor show a similar average crust thickness of about 60 km below the highlands and 30 below the lowlands (Figures 2b and 2d), which is similar to the 58 km and 32 km, respectively, estimated by the combined analysis of Mars Orbiter Laser Altimeter topography and Mars Global Surveyor gravity data [*Neumann et al.*, 2004]. Another consequence of such a giant impact is a residual asymmetrical thermal anomaly inside Mars that develops into active volcanism in the southern hemisphere (Figure 1h), with a few isolated plumes that might even have contributed to form minor volcanic features in the northern lowlands [*Garvin et al.*, 2000], but not enough to produce crust comparable to the highlands (see supporting information Movie S3). Further details on the development of crustal thickness and surface topography over time can be found in Figures S1 and S2.
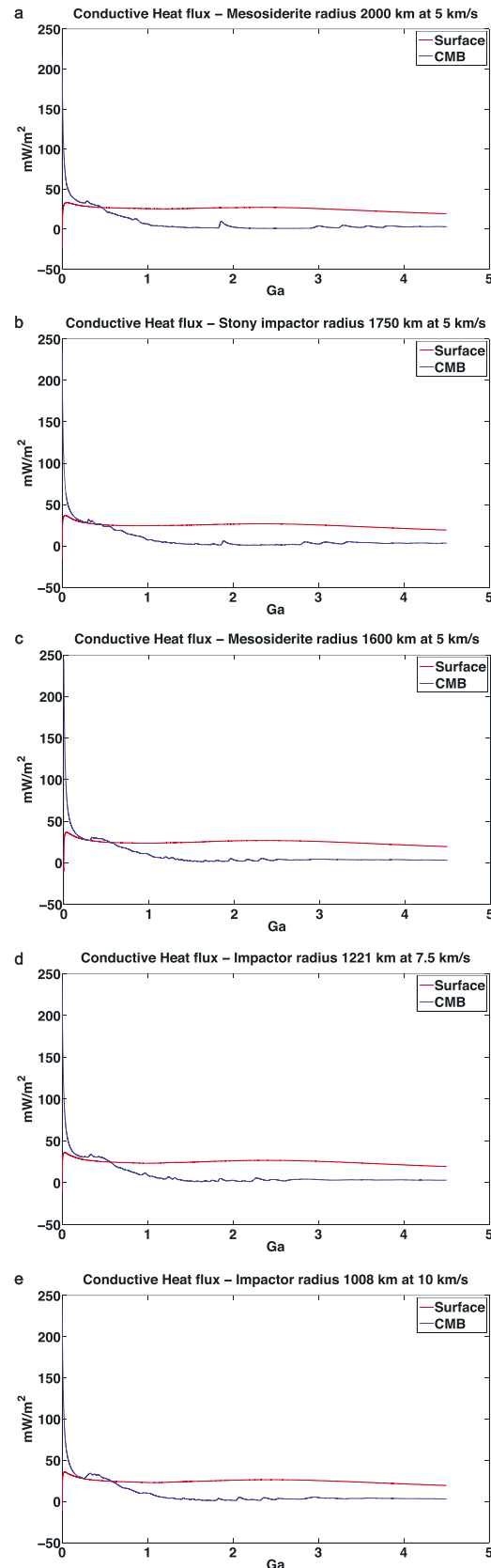
Visualization of mantle temperature isosurfaces during the long-term evolution phase (supporting information Movie S2) reveals several mantle plumes in the southern region 157 Ma after the impact (Figure 2k), which slowly migrate toward the South Pole of Mars due to the large-scale flow induced by the impact thermal anomaly: upwelling in the southern polar region results in lateral flow toward the South Pole in the deep mantle and away from the South Pole in the shallow mantle. With time, new plumes form in the equatorial region at an angular distance of about 20° from the first ones and also migrate toward the pole (Figure 2l, 290 Ma after the impact), a process that is also continuing 388 Ma after the impact (Figure 2m).

The global CMB heat flux following the giant impact drops from 100 to 60 mW/m^2 in the first 0.1 Ga, to 50 mW m^{-2} in the first 0.4 Ga, and to 20 mW m^{-2} by 0.6 Ga, then declining to 10 mW m^{-2} around 1 Ga (Figure 3). This large drop is sufficient to shut off the geodynamo without the assistance of additional impacts (as proposed by *Roberts et al.* [2009]) or any other special mechanism being necessary. Quantitatively, a lower bound on core heat flow for a planetary dynamo to operate is given by the heat conducted down the core adiabat. For Earth this has recently been estimated to be 10–16 TW [*de Koker et al.*, 2012; *Gomi et al.*, 2013; *Pozzo et al.*, 2012], corresponding to a flux of 66–105 mW m^{-2}. Scaling to the lower gravity of Mars, this leads to a critical heat flux somewhere in the range 20–40 mW m^{-2}, which is passed at around 4 Ga in our simulations. This timeline is thus consistent with the 4.15–4.07 Ga estimated from the map of the crustal magnetic field [*Lillis et al.*, 2008], although there is some uncertainty in the absolute age. It is also consistent with the time of changes in the Mars surface environment inferred by mineral alteration [*Bibring et al.*, 2006], which may be linked to loss of the atmosphere following magnetic field shutdown. The surface global average heat flux, after an initial peak of 30–35 mW m^{-2}, decreases to 20 mW m^{-2}. This is consistent with the global average heat flux values estimated from lithospheric flexures for the present day, which indicate 14−22 mW m^{-2} [*Ruiz et al.*, 2010], with the lower end estimated for Isidis [*Dehant et al.*, 2012].

4. Discussion

Mars shows no evident traces of plate tectonics and the geological record visible on the surface dates back to its most ancient times [*Carr and Head*, 2010]. Although *Sleep* [1994] proposed a brief episode of plate tectonics in the northern hemisphere, no evidence of any relic subduction zone has been found which, together with concerns about the timescale involved, make this scenario unlikely [*Watters et al.*, 2007]. Volcanic activity was clearly important early in its history; for example, a recent analysis of High Resolution

Figure 2. (a) Surface topography 4.5 Ga after the southern polar giant impact (SPGI) at 5 km s^{-1} for the impactor of 2000 km radius. The *y* axis indicates the latitude, the *x* axis the longitude, and the color bar the altimetry, which is shifted about 3 km above Mars values due to a different reference level. (b) Crustal thickness distribution formed by the 2000 km impactor, which is around 50 km below the highlands and around 30 km below the lowlands, values consistent with the average crustal thicknesses estimated through gravity measurements [*Neumann et al.*, 2004]. (c) Surface topography 4.5 Ga after SPGI at 5 km s^{-1} for the impactor of 1600 km of radius; the values are comparable to those obtained for the 2000 km impactor. (d) Crustal thickness distribution formed by the 1600 km impactor. (e) Surface topography 4.5 Ga after SPGI at 7.5 km s^{-1} for the impactor of 1221 km of radius. (f) Crustal thickness distribution formed by the 1221 km impactor. (g) Surface topography 4.5 Ga after SPGI at 10 km s^{-1} for the impactor of 1008 km of radius. (h) Crustal thickness distribution formed by the 1008 km impactor. (i) Surface topography 4.5 Ga after SPGI at 5 km s^{-1} for the stony impactor of 1750 km of radius. (j) Crustal thickness distribution formed by the 1750 km impactor. View from the south polar direction of the 2000 K temperature isosurface: (k) 157 Ma after the impact, (l) 290 Ma after the impact, and (m) 388 Ma after the impact with a siderite of 1600 km. These show mantle plumes converging toward the South Pole (center of the image) as well as new plumes forming increasingly further from the South Pole.

Imaging Science Experiment (HiRISE) images of Valles Marineris has led to the hypothesis that it formed through erosion by lava flows rather than tectonic force and that the putative shorelines in Chryse Planitia are the lava flow fronts coming from Valles Marineris [*Leone*, 2014]. The lack of significant ongoing volcanic activity, such as that observed on Earth today, and the asymmetric position of the volcanic features, mostly located in the southern hemisphere starting from the equator, indicate that internal heat sources (primordial and radioactive) are insufficient to sustain activity at global scale over geological time. This conclusion is expected given the small size of Mars relative to Earth [*Breuer and Moore*, 2007].

According to the geochronostratigraphic map of Mars [*Tanaka et al.,* 2013], the oldest volcanic features are located between the equator and the southern polar region, in particular upper Noachian terrains at the equator. The geologic ages estimated for the volcanic features would thus suggest a progressive sequence of emplacement in space and time from the equator to the South Pole, consistent with the appearance of new plumes progressively closer to the equator in our model. The majority of the volcanic provinces are of Hesperian age, except the South Pole and the Tharsis and Elysium Rises that are indicated as Amazonian. The young age inferred might likely be related to the geological processes that the volcanic centers underwent during their history, volcanic, aqueous, glacial, and aeolian processes that continued (volcanic) or started (aqueous, glacial, and aeolian) after the original time of emplacement. For example, although its latest lava flows appear young, the bulk material of Olympus Mons might date back to Hesperian or Noachian times [*Isherwood et al.*, 2013].

We find that a larger impactor is needed in these 3-D simulations than was required in the previous 2-D cylindrical calculations [*Golabek et al.*, 2011], which is because the ratio of impactor mass to target mass scales differently with dimensionality, and also in the analytical study of *Reese et al.* [2010], which is mainly because they assumed a higher impact velocity.

Figure 3. Surface (red line) and core-mantle boundary (blue line) heat flux evolution along the whole history of Mars for the different impactors of mesosideritic composition: (a) 2000 km, (b) 1750 km, (c) 1600 km, (d) 1221 km, and (e) 1008 km. No particular variation in the heat flux trend is observed for the different impactors, the thermal evolution of the planet is neither affected by the size of the impactor nor by the strength of the initial thermal anomaly. The different thermal anomalies are evidently dissipated by different degrees of volcanism during the initial phase, while the long-term thermal evolution of the planet follows the normal decay of the radiogenic heating.

5. Conclusions

Our model results indicate that the south polar giant impact (SPGI) is a viable hypothesis to explain the origin of the crustal dichotomy and can explain: (a) the origin and the morphology of the Martian dichotomy; (b) the distribution, the timing, and the onset of the volcanic features; and (c) the decline of the magnetic field. Our assumptions and consequent results are consistent with a range of geochemical, geological, volcanological, and astronomical results that are briefly summarized here: (i) a short time for core formation of 5–7 Ma after CAI, dependent on the size of the impactor (the larger the size the shorter the time), which is within the 3–15 Ma estimated by the geochemistry; (ii) extent of the highlands in latitude consistent with that observed on the map of Mars; (iii) crustal thickness consistent with that inferred from gravity measurements; (iv) presence of significant volcanism mainly at the equator and in the southern hemisphere; (v) migration of mantle plumes in the southern hemisphere; (vi) decline time of the transient magnetic field consistent with the observation of the magnetic anomalies on both highlands and lowlands; (vii) decline time of the volcanism consistent with geological observations; (viii) impactor velocity similar to the escape velocity of the target; (ix) impact velocity avoiding disruption of the target; and (x) dichotomy match with either impactor's mesosideritic or sideritic composition.

We consider the impact time of 4 Ma after CAI as a lower bound for the dichotomy formation—the giant impact could have happened any time between 4 and 15 Ma after CAI, but not later as it might raise a problem with the geochemistry of the mantle-core differentiation. If the giant impact occurred later, it might have geochemically reequilibrated the core and mantle, thus altering the above mentioned times, although this is not necessarily the case—for large impacts, the impactor core can drop quite rapidly into the target core (scenario C in *Nimmo and Agnor* [2006]).

Further refinement of the available models could still be possible thanks to the seismic and thermal data that will come from the InSight Mission to Mars, providing new information on the size of the planet's core and its surface thermal flux, and to the observation of the distribution of the volcanic centers on the surface.

References

Agnor, C. B., R. M. Canup, and H. F. Levison (1999), On the character and consequences of large impacts in the late stage of terrestrial planet formation, *Icarus*, *142*(1), 219–237, doi:10.1006/Icar.1999.6201.

Andrews-Hanna, J. C., M. T. Zuber, and W. B. Banerdt (2008), The Borealis basin and the origin of the Martian crustal dichotomy, *Nature*, *453*(7199), 1212–1227, doi:10.1038/Nature07011.

Bibring, J. P., et al. (2006), Global mineralogical and aqueous Mars history derived from OMEGA/Mars Express data, *Science*, *312*(5772), 400–404, doi:10.1126/Science.1122659.

Breuer, D., and W. B. Moore (2007), Dynamics and thermal history of the terrestrial planets, the Moon, and Io, in *Treatise on Geophysics*, edited by T. Spohn, Elsevier B. V., Amsterdam.

Carr, M. H., and J. W. Head (2010), Geologic history of Mars, *Earth Planet. Sci. Lett.*, *294*(3–4), 185–203, doi:10.1016/J.Epsl.2009.06.042.

de Koker, N., G. Steinle-Neumann, and V. Vlcek (2012), Electrical resistivity and thermal conductivity of liquid Fe alloys at high P and T, and heat flux in Earth's core, *Proc. Natl. Acad. Sci. U.S.A.*, *109*(11), 4070–4073, doi:10.1073/pnas.1111841109.

Dehant, V., et al. (2012), Future Mars geophysical observatories for understanding its internal structure, rotation, and evolution, *Planet. Space Sci.*, *68*(1), 123–145, doi:10.1016/J.Pss.2011.10.016.

Frey, H., and R. A. Schultz (1988), Large impact basins and the mega-impact origin for the crustal dichotomy on Mars, *Geophys. Res. Lett.*, *15*(3), 229–232, doi:10.1029/GL015i003p00229.

Frey, H. V. (2006), Impact constraints on, and a chronology for, major events in early Mars history, *J. Geophys. Res.*, *111*, E08S91, doi:10.1029/2005JE002449.

Garvin, J. B., S. E. H. Sakimoto, J. J. Frawley, C. C. Schnetzler, and H. M. Wright (2000), Topographic evidence for geologically recent near-polar volcanism on Mars, *Icarus*, *145*(2), 648–652, doi:10.1006/Icar.2000.6409.

Gerya, T. V., and D. A. Yuen (2007), Robust characteristics method for modelling multiphase visco-elasto-plastic thermo-mechanical problems, *Phys. Earth Planet. In.*, *163*(1–4), 83–105, doi:10.1016/J.Pepi.2007.04.015.

Golabek, G. J., T. Keller, T. V. Gerya, G. Z. Zhu, P. J. Tackley, and J. A. D. Connolly (2011), Origin of the Martian dichotomy and Tharsis from a giant impact causing massive magmatism, *Icarus*, *215*(1), 346–357, doi:10.1016/J.Icarus.2011.06.012.

Goldstein, J. I., E. R. D. Scott, and N. L. Chabot (2009), Iron meteorites: Crystallization, thermal history, parent bodies, and origin, *Chem. Erde-Geochem.*, *69*(4), 293–325, doi:10.1016/J.Chemer.2009.01.002.

Gomi, H., K. Ohta, K. Hirose, S. Labrosse, R. Caracas, M. J. Verstraete, and J. W. Hernlund (2013), The high conductivity of iron and thermal evolution of the Earth's core, *Phys. Earth Planet. Inter. (Netherlands)*, *224*, 88–103, doi:10.1016/j.pepi.2013.07.010.

Isherwood, R. J., L. M. Jozwiak, J. C. Jansen, and J. C. Andrews-Hanna (2013), The volcanic history of Olympus Mons from paleo-topography and flexural modeling, *Earth Planet. Sci. Lett.*, *363*, 88–96, doi:10.1016/J.Epsl.2012.12.020.

Jacobsen, S. B. (2005), The Hf-wisotopic system and the origin of the Earth and Moon, *Annu. Rev. Earth Planet. Sci.*, *33*, 531–570, doi:10.1146/Annurev.Earth.33.092203.122614.

Keller, T., and P. J. Tackley (2009), Towards self-consistent modeling of the Martian dichotomy: The influence of one-ridge convection on crustal thickness distribution, *Icarus*, *202*(2), 429–443, doi:10.1016/J.Icarus.2009.03.029.

Le Feuvre, M., and M. A. Wieczorek (2008), Nonuniform cratering of the terrestrial planets, *Icarus*, *197*(1), 291–306, doi:10.1016/J.Icarus.2008.04.011.

Leinhardt, Z. M., and D. C. Richardson (2002), N-body simulations of planetesimal evolution: Effect of varying impactor mass ratio, *Icarus*, *159*(2), 306–313, doi:10.1006/Icar.2002.6909.

Leone, G. (2014), A network of lava tubes as the origin of Labyrinthus Noctis and Valles Marineris on Mars, *J. Volcanol. Geotherm. Res.*, *277*, 1–8.

Lillis, R. J., H. V. Frey, M. Manga, D. L. Mitchell, R. P. Lin, M. H. Acuna, and S. W. Bougher (2008), An improved crustal magnetic field map of Mars from electron reflectometry: Highland volcano magmatic history and the end of the Martian dynamo, *Icarus*, *194*(2), 575–596, doi:10.1016/J.Icarus.2007.09.032.

Marinova, M. M., O. Aharonson, and E. Asphaug (2008), Mega-impact formation of the Mars hemispheric dichotomy, *Nature*, *453*(7199), 1216–1219, doi:10.1038/Nature07070.

McCoy, T. J., et al. (2011), Group IVA irons: New constraints on the crystallization and cooling history of an asteroidal core with a complex history, *Geochim. Cosmochim. Acta*, *75*(22), 6821–6843, doi:10.1016/J.Gca.2011.09.006.

Monteux, J., N. Coltice, F. Dubuffet, Y. Ricard (2007), Thermo-mechanical adjustment after impacts during planetary growth, *Geophys. Res. Lett.*, *34*, L24201, doi:10.1029/2007GL031635.

Morishima, R., J. Stadel, and B. Moore (2010), From planetesimals to terrestrial planets: N-body simulations including the effects of nebular gas and giant planets, *Icarus*, *207*(2), 517–535, doi:10.1016/J.Icarus.2009.11.038.

Neumann, G. A., M. T. Zuber, M. A. Wieczorek, P. J. McGovern, F. G. Lemoine, and D. E. Smith (2004), Crustal structure of Mars from gravity and topography, *J. Geophys. Res.*, *109*, E08002, doi:10.1029/2004JE002262.

Nimmo, F., and C. B. Agnor (2006), Isotopic outcomes of N-body accretion simulations: Constraints on equilibration processes during large impacts from HfAV observations, *Earth Planet. Sci. Lett.*, *243*(1–2), 26–43, doi:10.1016/J.Epsl.2005.12.009.

Nimmo, F., S. D. Hart, D. G. Korycansky, and C. B. Agnor (2008), Implications of an impact origin for the Martian hemispheric dichotomy, *Nature*, *453*(7199), 1220–1232, doi:10.1038/Nature07025.

Ockert-Bell, M. E., B. E. Clark, M. K. Shepard, R. A. Isaacs, E. A. Cloutis, S. Fornasier, and S. J. Bus (2010), The composition of M-type asteroids: Synthesis of spectroscopic and radar observations, *Icarus*, *210*(2), 674–692, doi:10.1016/J.Icarus.2010.08.002.

Osinski, G. R., and E. Pierazzo (2013), The isobaric core, in *Impact Cratering*, 1st ed., edited by G. R. Osinski and E. Pierazzo, 38 pp., Wiley and Blackwell, Chichester, England.

Pierazzo, E., and H. J. Melosh (2000), Melt production in oblique impacts, *Icarus*, *145*(1), 252–261.

Pozzo, M., C. Davies, D. Gubbins, and D. Alfe (2012), Thermal and electrical conductivity of iron at Earth's core conditions, *Nature (UK)*, *485*(7398), 355–358, doi:10.1038/nature11031.

Reese, C. C., and V. S. Solomatov (2006), Fluid dynamics of local Martian magma oceans, *Icarus*, *184*(1), 102–120, doi:10.1016/J.Icarus.2006.04.008.

Reese, C. C., and V. S. Solomatov (2010), Early Martian dynamo generation due to giant impacts, *Icarus*, *207*(1), 82–97, doi:10.1016/J.Icarus.2009.10.016.

Reese, C. C., C. P. Orth, and V. S. Solomatov (2010), Impact origin for the Martian crustal dichotomy: Half emptied or half filled?, *J. Geophys. Res.*, *115*, E05004, doi:10.1029/2009JE003506.

Reese, C. C., C. P. Orth, and V. S. Solomatov (2011), Impact megadomes and the origin of the Martian crustal dichotomy, *Icarus*, *213*(2), 433–442, doi:10.1016/J.Icarus.2011.03.028.

Righter, K., and C. K. Shearer (2003), Magmatic fractionation of Hf and W: Constraints on the timing of core formation and differentiation in the Moon and Mars, *Geochim. Cosmochim. Acta*, *67*(13), 2497–2507.

Roberts, J. H., R. J. Lillis, and M. Manga (2009), Giant impacts on early Mars and the cessation of the Martian dynamo, *J. Geophys. Res.*, *114*, E04009, doi:10.1029/2008JE003287.

Ruiz, J., V. Lopez, and J. M. Dohm (2010), The present-day thermal state of Mars, *Icarus*, *207*(2), 631–637, doi:10.1016/J.Icarus.2010.01.016.

Senshu, H., K. Kuramoto, and T. Matsui (2002), Thermal evolution of Mars, *J. Geophys. Res.*, *107*(E12), 5118, doi:10.1029/2001JE001819.

Sleep, N. H. (1994), Martian plate-tectonics, *J. Geophys. Res.*, *99*(E3), 5639–5655, doi:10.1029/94JE00216.

Solomon, S. C., et al. (2005), New perspectives on ancient Mars, *Science*, *307*(5713), 1214–1220.

Sramek, O., L. Milelli, Y. Ricard, and S. Labrosse (2012), Thermal evolution and differentiation of planetesimals and planetary embryos, *Icarus*, *217*(1), 339–354.

Stewart, S. T., and Z. M. Leinhardt (2012), Collisions between gravity-dominated bodies. II. The diversity of impact outcomes during the end stage of planet formation, *Astrophys. J.*, *751*(1), doi:10.1088/0004-637x/751/1/32.

Tackley, P. J. (2008), Modelling compressible mantle convection with large viscosity contrasts in a three-dimensional spherical shell using the yin-yang grid, *Phys. Earth Planet. In.*, *171*(1–4), 7–18, doi:10.1016/J.Pepi.2008.08.005.

Tanaka, K. L., J. A. P. Rodriguez, J. A. Skinner, M. C. Bourke, C. M. Fortezzo, K. E. Herkenhoff, E. J. Kolb, and C. H. Okubo (2008), North polar region of Mars: Advances in stratigraphy, structure, and erosional modification, *Icarus*, *196*(2), 318–358, doi:10.1016/J.Icarus.2008.01.021.

Tanaka, K. L., S. J. Robbins, C. M. Fortezzo, J. A. Skinner, and T. M. Hare (2013), The digital global geologic map of Mars: Chronostratigraphic ages, topography and crater morphologic characteristics, and updated resurfacing history, *Planet. Space Sci.*, doi:10.1016/j.pss.2013.03.006.

Tonks, W. B., and H. J. Melosh (1993), Magma ocean formation due to giant impacts, *J. Geophys. Res.*, *98*(E3), 5319–5333, doi:10.1029/92JE02726.

Watters, T. R., P. J. McGovern, and P. I. Rossman (2007), Hemispheres apart: The crustal dichotomy on Mars, *Annu. Rev. Earth Planet. Sci.*, *35*, 621–652, doi:10.1146/annurev.earth.35.031306.140220.

Wilhelms, D. E., and S. W. Squyres (1984), The Martian hemispheric dichotomy may be due to a giant impact, *Nature*, *309*(5964), 138–140, doi:10.1038/309138a0.

Zhong, S. J., and M. T. Zuber (2001), Degree-1 mantle convection and the crustal dichotomy on Mars, *Earth Planet. Sci. Lett.*, *189*(1–2), 75–84, doi:10.1016/S0012-821x(01)00345-4.